

Article

Morphology Design and Fabrication of Bio-Inspired Nano-MgO–Mg(OH)₂ via Vapor Steaming to Enable Bulk CO₂ Diffusion and Capture

Hasanthi L. Senevirathna, Shunnian Wu, W. P. Cathie Lee  and Ping Wu * 

Entropic Interface Group, Engineering Product Development, Singapore University of Technology and Design, 8 Somapah Road, Singapore 487372, Singapore; hasanthi_senevirathna@mymail.sutd.edu.sg (H.L.S.); shunnian_wu@sutd.edu.sg (S.W.); cathie_lee@sutd.edu.sg (W.P.C.L.)

* Correspondence: wuping@sutd.edu.sg

Abstract: The absorption of CO₂ on MgO is being studied in depth in order to enhance carbon engineering. Production of carbonate on MgO surfaces, such as MgCO₃, for example, has been shown to hinder further carbon lattice transit and lower CO₂ collecting efficiency. To avoid the carbonate blocking effect, we mimic the water harvesting nano-surface systems of desert beetles, which use alternate hydrophobic and hydrophilic surface domains to collect liquid water and convey condensed droplets down to their mouths, respectively. We made CO₂-philic MgO and CO₂-phobic Mg(OH)₂ nanocomposites from electrospun nano-MgO by vapor steaming for 2–20 min at 100 °C. The crystal structure, morphology, and surface properties of the produced samples were instrumentally characterized using XRD, SEM, XPS, BET, and TGA. We observed that (1) fiber morphology shifted from hierarchical particle and sheet-like structures to flower-like structures, and (2) CO₂ capture capacity shifted by around 25%. As a result, the carbonate production and breakdown processes may be managed and improved using vapor steaming technology. These findings point to a new CO₂ absorption technique and technology that might pave the way for more CO₂ capture, mineralization, and fuel synthesis options.

Keywords: MgO–Mg(OH)₂ composites; CO₂ adsorption; hydration; electrospinning



Citation: Senevirathna, H.L.; Wu, S.; Lee, W.P.C.; Wu, P. Morphology Design and Fabrication of Bio-Inspired Nano-MgO–Mg(OH)₂ via Vapor Steaming to Enable Bulk CO₂ Diffusion and Capture. *Materials* **2022**, *15*, 680. <https://doi.org/10.3390/ma15020680>

Academic Editor: Paula Teixeira

Received: 20 December 2021

Accepted: 14 January 2022

Published: 17 January 2022

Publisher's Note: MDPI stays neutral with regard to jurisdictional claims in published maps and institutional affiliations.



Copyright: © 2022 by the authors. Licensee MDPI, Basel, Switzerland. This article is an open access article distributed under the terms and conditions of the Creative Commons Attribution (CC BY) license (<https://creativecommons.org/licenses/by/4.0/>).

1. Introduction

The increasing amount of anthropogenic carbon dioxide (CO₂) in the atmosphere, which contributes to global climate change, has necessitated the development of new technologies and materials. Efforts to produce effective CO₂ capture materials have been made in large numbers [1,2]. Environmentally friendly nanomaterials have recently become vital in a variety of research and development domains. Magnesium oxide (MgO) and magnesium hydroxide (Mg(OH)₂) are two of the most environmentally friendly materials when compared to other materials [3–5]. For properties such as flame resistance, dielectric resistance, and mechanical strength; and micro structural properties such as porosity, large surface area catalysis, acid–base sites, and gas adsorption, MgO is well received in industrial applications such as ceramics, cement, and water treatments [2,5–11]. At intermediate temperatures, CO₂ adsorbents based on MgO have been identified as promising. As a result, numerous researchers have looked at using magnesium oxide to trap CO₂. For instance, MgO-based adsorbents for CO₂ capture produced using diverse techniques and under varied circumstances were recently evaluated by Hu et al. [1] and Ruhaimi et al. [12]. Elvira et al. [13] reported 1.61 wt.% of CO₂ capture capacity for MgO sorbent generated by solution–combustion and ball milling at 25 °C. MgO produced using the template approach at 25 °C was examined by Bhagiyalakshmi et al. [14], who found roughly 8 wt.%. Ho et al. [15] reported 30 wt.% mesoporous MgO produced using the aerogel technique at 30 °C.

One of the most remarkable properties of $\text{Mg}(\text{OH})_2$ is its wide range of morphological shapes, which include needles, tubes, fibers, platelets, rods, and even flowers or valleys, among many other [16–18]. Methods for producing $\text{Mg}(\text{OH})_2$ include precipitation of a magnesium salt with an alkaline solution, the sol–gel technique, microwave-assisted approach synthesis, hydrothermal synthesis, and ammonia gas bubbling reactors. The MgO hydration approach, on the other hand, is thought to be one of the most cost-effective to date [2,19,20]. Many factors influence the hydration process, including MgO characteristics, external force environment, hydration temperature, and nucleation site. As a result, in order to obtain $\text{Mg}(\text{OH})_2$ with the desired characteristics, the reaction parameters of MgO hydration must be carefully controlled. Xing et al. [21] investigated the hydration of various active MgO under uncontrolled and ultrasonic circumstances, where the MgO hydration was governed by the main dissolving and precipitation processes at temperatures below 90°C . Thomas et al. [22] investigated the hydration kinetics of MgO to $\text{Mg}(\text{OH})_2$ in the cement industry. The bulk of these research studies, however, does not emphasize the use of MgO hydration for CO_2 collection.

Chemical adsorption of CO_2 by MgO results in the formation of a MgCO_3 layer at the surface shell, which inhibits CO_2 molecules from diffusing into the core MgO regions through the MgCO_3 shell. As a result, the CO_2 collection capability is significantly lower than expected by theory. The Namib desert beetle's effective water capture system is said to be made up of an interwoven water capture zone with high water adsorption and a water transport region with low water adsorption [23,24]. We designed our MgO – $\text{Mg}(\text{OH})_2$ composites to have an interweaved CO_2 capture region dominated by MgO , and a CO_2 diffusion region dominated by $\text{MgO}/\text{Mg}(\text{OH})_2$ interfaces. This was inspired by the interwoven composite. The CO_2 that has been physically adsorbed by MgO can diffuse into the inner layers and then be chemically adsorbed by the inner MgO . Furthermore, H_2O steam [25] may provide an additional CO_2 diffusion mechanism. As a result, in order to collect CO_2 efficiently at room temperature, our CO_2 capture device employs CO_2 -philic (MgO) and CO_2 -phobic ($\text{Mg}(\text{OH})_2$) domains to mimic the water harvesting mechanism of desert beetles [23]. We used water vapor steaming at 100°C to hydrate MgO and create $\text{Mg}(\text{OH})_2$ in electrospun MgO powders to create MgO – $\text{Mg}(\text{OH})_2$ composites. The crystal structure, morphology, and surface characteristics of the generated samples were examined using XRD, SEM, XPS, BET, and TGA. Thermodynamic and quantum mechanism models were created to aid in the analysis of the experiments.

2. Materials and Methods

2.1. Materials

For sample synthesis, analytical grade glacial acetic acid 99.8% was purchased from Scharlau (Barcelona, Spain). Analytical grade polyvinyl alcohol (PVA) (molecular weight 89,000–98,000, 99+% hydrolyzed) and $\text{Mg}(\text{OH})_2 \geq 99\%$ (BioUltra) were purchased from Sigma-Aldrich (Saint Louis, MO, USA). All the chemicals were utilized without further purification. Deionized water ($18\text{ M}\Omega\cdot\text{cm}$) was used in all the experimental works in this study.

2.2. Methods

The precursor solution for electrospinning was prepared by dissolving 0.25 g $\text{Mg}(\text{OH})_2$ in 5 mL acetic acid under sonication in a water bath at 50°C for 1 h until a clear solution was obtained. Then the aqueous PVA (5% *w/w*) solution, 0.750 mL, was added to the clear solution and further sonicated in a water bath at 50°C for 30 min to eliminate any precipitation. The electrospinning was carried out in a similar manner as we reported in our earlier study [26]. The collected layer of nanofibers was kept drying at 60°C for 48 h. The oven dried samples were then collected as solidified flakes and calcined in a muffle furnace (Nabertherm) at 350°C for 1 h at a rate of 2°C min^{-1} naturally cooling to room temperature. The samples were collected and ground using a motor and pestle to obtain a fine powder.

The fine powder obtained was then spread on a flat ceramic crucible and kept inside a super heating steam oven at 100 °C. Five samples were prepared by varying the steam exposure time (2-min, 5-min, 10-min, 15-min, and 20-min), and one sample was kept without exposing to steam (no-steam). The steamed samples were then kept at 30 °C for 24 h for drying.

3. Characterization

Surface structure and morphology were examined by using field emission scanning electron microscopy (FE-SEM) (JEOL JSM-7600F, Jeol, Tokyo, Japan). X-ray diffraction (XRD) analysis was carried out using a Bruker D8 Advance X-ray diffractometer with Cu-K radiation of 1.54. The scanning angle was adjusted from 10° to 70° with the X-ray generator running at an applied voltage of 40 kV and a current of 25 mA. Brunauer–Emmett–Teller (BET) surface area analysis was performed by using a Micrometrics ASAP 2020 system. A BET test was conducted at 120 °C using 0.1 g of powder samples. X-ray photoelectron spectroscopy (XPS) was conducted using a Thermo Fisher Scientific Theta Probe (Thermo Fisher Scientific, Waltham, MA, USA) with a monochromatic Al K α radiation. Binding energies (BE) were determined by referencing to adventitious carbon C1s at 285.0 eV. Thermogravimetric analysis (TGA) of the samples for CO₂ capture was conducted using a TGA Q50 analyzer (TA Instruments, New Castle, DE, USA). TGA analysis was carried out by loading 5–7 mg of samples onto a platinum pan in the TGA unit. At the beginning of the TGA run, samples were pre-treated at 150 °C for 60 min under a flow of high purity N₂ (40 mL min⁻¹) with a ramp rate of 10 °C min⁻¹ to avoid errors originating from the pre-adsorbed atmospheric CO₂, water, and other impurities. Following that, the temperature was gradually reduced to 30 °C at a rate of 10 °C min⁻¹. At this stage, the gas was switched from N₂ to high purity CO₂ gas. CO₂ capture capacity for all samples was recorded for 1.5 h in TGA analysis under pure CO₂ environment. Furthermore, each sample's TGA measurement was repeated three times to ensure that it was repeatable. The calculated standard deviation was smaller than one in the identical set of conditions.

4. Results and Discussion

4.1. CO₂ Capture Capacity of Samples

The CO₂ adsorption capacity was measured using a Q50 TGA analyzer for each sample. The samples with weights in the range of 5 to 7 mg were analyzed at 30 °C with a constant flow of high purity CO₂ for 1.5 h. The CO₂ levels in TGA measurements approached a plateau when the testing duration reached 1.5 h, and adsorption arrived at the maximum CO₂ capture capacity [27]. Figure 1 shows the TGA data obtained for the samples.

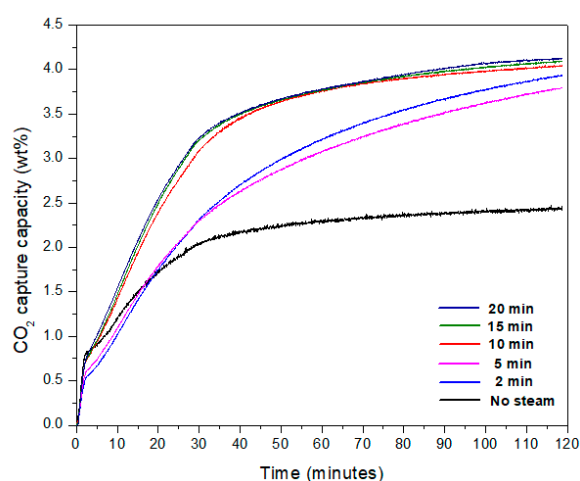


Figure 1. TGA data for electrospun samples before steam exposure (no-steam) and after steam exposure for different time periods (2-min, 5-min, 10-min, 15-min, and 20-min).

The CO₂ collection capability of the samples is summarized in Figure 1. The no-steam sample was the sample as-prepared before being exposed to steam at 100 °C. We compared our outcomes before (no-steam) and after (steam) steam exposure (2-min, 5-min, 10-min, 15-min, and 20-min). Figure 1 shows that when samples were subjected to steam, CO₂ capture was higher than when samples were not exposed to steam (no-steam sample). The CO₂ capacity of the no-steam sample was 2.43 wt.%, compared to 4.12 wt.% for the sample subjected to steam for 20 min. As compared to the no-steam sample, the capture capacity nearly doubled after 20 min of steam exposure. The production of Mg(OH)₂ may increase surface area, allowing for better CO₂ collection. Furthermore, the presence of H₂O may improve CO₂ collection even more [25]. In addition, each sample's data was replicated three times to ensure that it was repeatable. The computed standard deviation was smaller than 1 in the identical conditions.

4.2. Structural and Morphological Characterization

The structural characterization of the samples was carried out by XRD analysis. Figure 2 shows the results obtained. The results showed that the before steam sample only indicated the MgO where the main 2θ peaks of the MgO, namely 36.9°, 42.9°, and 62.3°, were consistent with (111), (200), and (220) lattice planes, respectively, were in good agreement with MgO (ICDD 00-045-0946). After the steam exposure, the peak related to Mg(OH)₂ emerged. The steam samples showed both MgO- and Mg(OH)₂-related peaks. The main 2θ peaks for the steamed samples of Mg(OH)₂, namely 18.5°, 37.9°, 50.7°, and 58.6°, were consistent with (001), (101), (102), and (110) lattice planes, respectively, in good agreement with Mg(OH)₂ (ICDD 00-044-1482). They also showed the MgO 2θ peaks 42.9° and 62.3° were consistent with (200) and (220) lattice planes. As shown in Figure 2, before the sample was exposed to steam (no-steam sample), only MgO was present, and after the samples were exposed to steam at 100 °C for 2-min, 5-min, 10-min, 15-min, and 20-min, the MgO-Mg(OH)₂ composite structure was formed. The intensity of the peaks related to Mg(OH)₂ increased as the steam exposure time increased, while the intensity of the peaks related to MgO decreased as the steam exposure time increased.

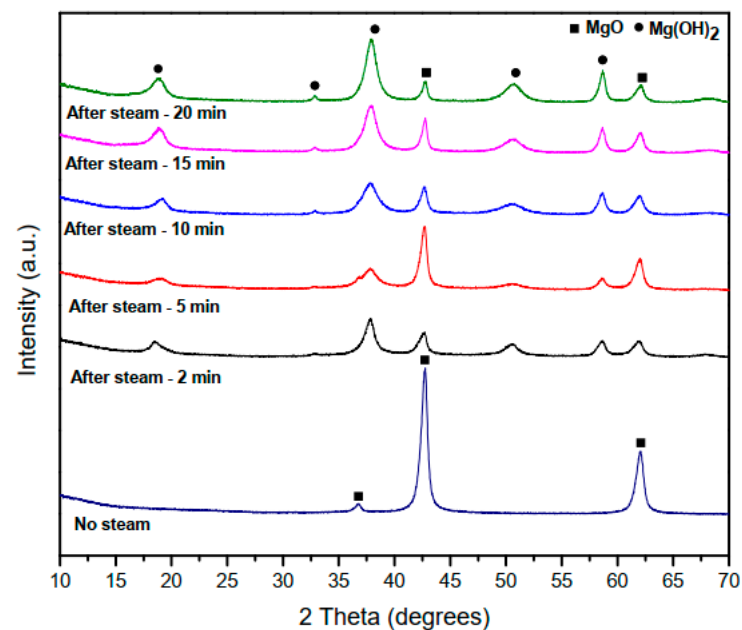


Figure 2. A comparison of XRD patterns for samples before exposure to steam (no-steam) and after exposure to steam for 2-min, 5-min, 10-min, 15-min, and 20-min, at 100 °C.

The sample morphology was analyzed using SEM images, which are shown in Figure 3 below.

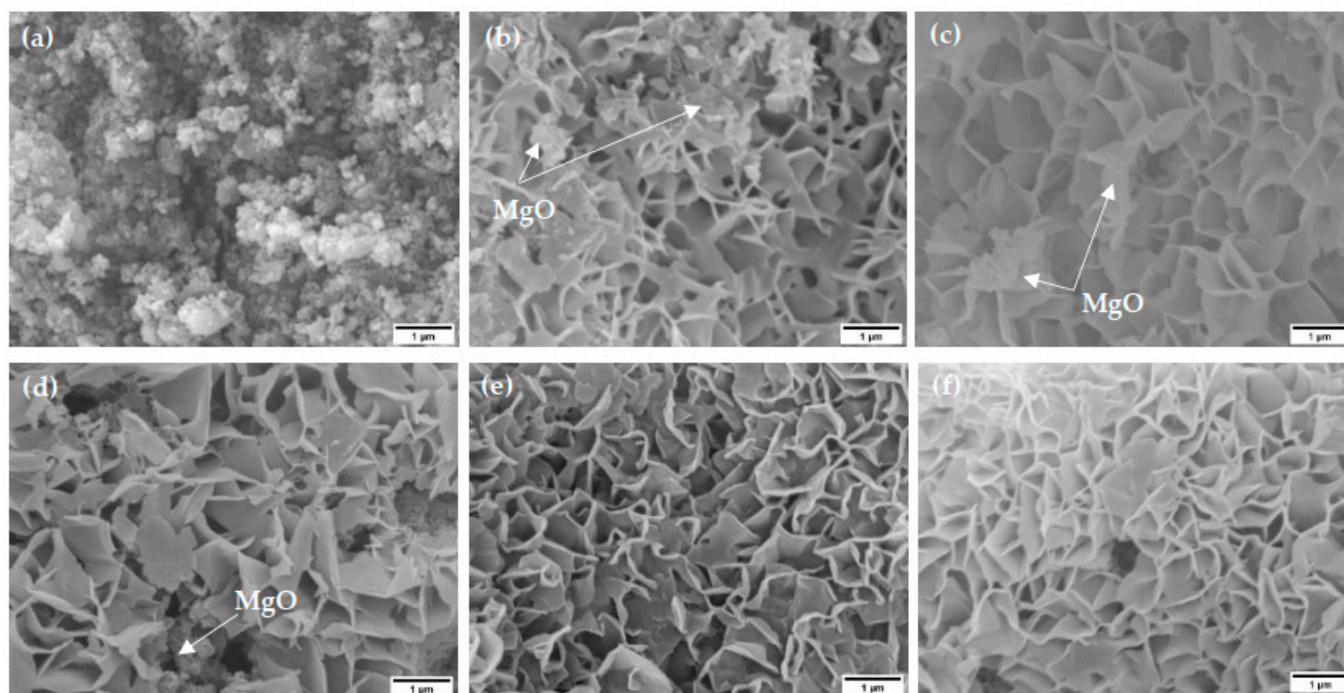


Figure 3. SEM images of electrospun MgO samples (a) before exposure to steam (no-steam) and after exposure to steam for (b) 2-min, (c) 5-min, (d) 10-min, (e) 15-min, and (f) 20-min at 100 °C.

The sample morphology before steam exposure (no-steam) in Figure 3a shows hierarchical particle and sheet-like structures. After steam exposure, flower-like structures could be observed, as shown in Figure 3b–f. The interlaced vertical nano-sheets of $\text{Mg}(\text{OH})_2$ were firmly and uniformly grown on the samples after different time periods of steam exposure (2-min, 5-min, 10-min, 15-min, and 20-min), with an average diameter of 100 nm. The uniformity of the structures increased as the steam exposure time increased. Unreacted MgO could be observed in the 2-min (Figure 3b), 5-min (Figure 3c), and 10-min (Figure 3d) steam exposed samples along with the $\text{Mg}(\text{OH})_2$ structures, respectively. However, at 15-min (Figure 3e) and 20-min (Figure 3f), there was more uniform flower-like structure formation in the scanned area.

The XPS analysis for the samples were carried out to further analyze the surface chemistry of the samples. A summary of the data obtained for the 2-min, 5-min, 10-min, 15-min, and 20-min steam samples is shown in Figure 4.

The XPS data showed the presence of MgO and $\text{Mg}(\text{OH})_2$ in the samples. The $\text{Mg}(\text{OH})_2$ appeared in the XPS data after 10 min of steaming. The no-steam sample showed the presence of a peak located at 531.75 eV. In comparison to this energy peak, it can be seen that the peaks related to Mg–O energy decreased the binding energy with increased steam exposure time. Additionally, in both the O 1s spectra and the Mg 2p spectra, where the samples were steamed for 10-min and above, there were the presence of adsorbed –OH groups. The O 1s spectra showed that the peaks related to –OH were derived from the chemisorbed –OH groups on the surface of MgO during steaming with binding energy values of 531.89 eV, 532.03 eV, and 531.89 eV for 10-min, 15-min, and 20-min steam exposed samples. It was seen that the peak intensities in the Mg 2p spectra increased with increased steaming time, indicating the improved formation of $\text{Mg}(\text{OH})_2$ due to the chemisorption of –OH in MgO [28].

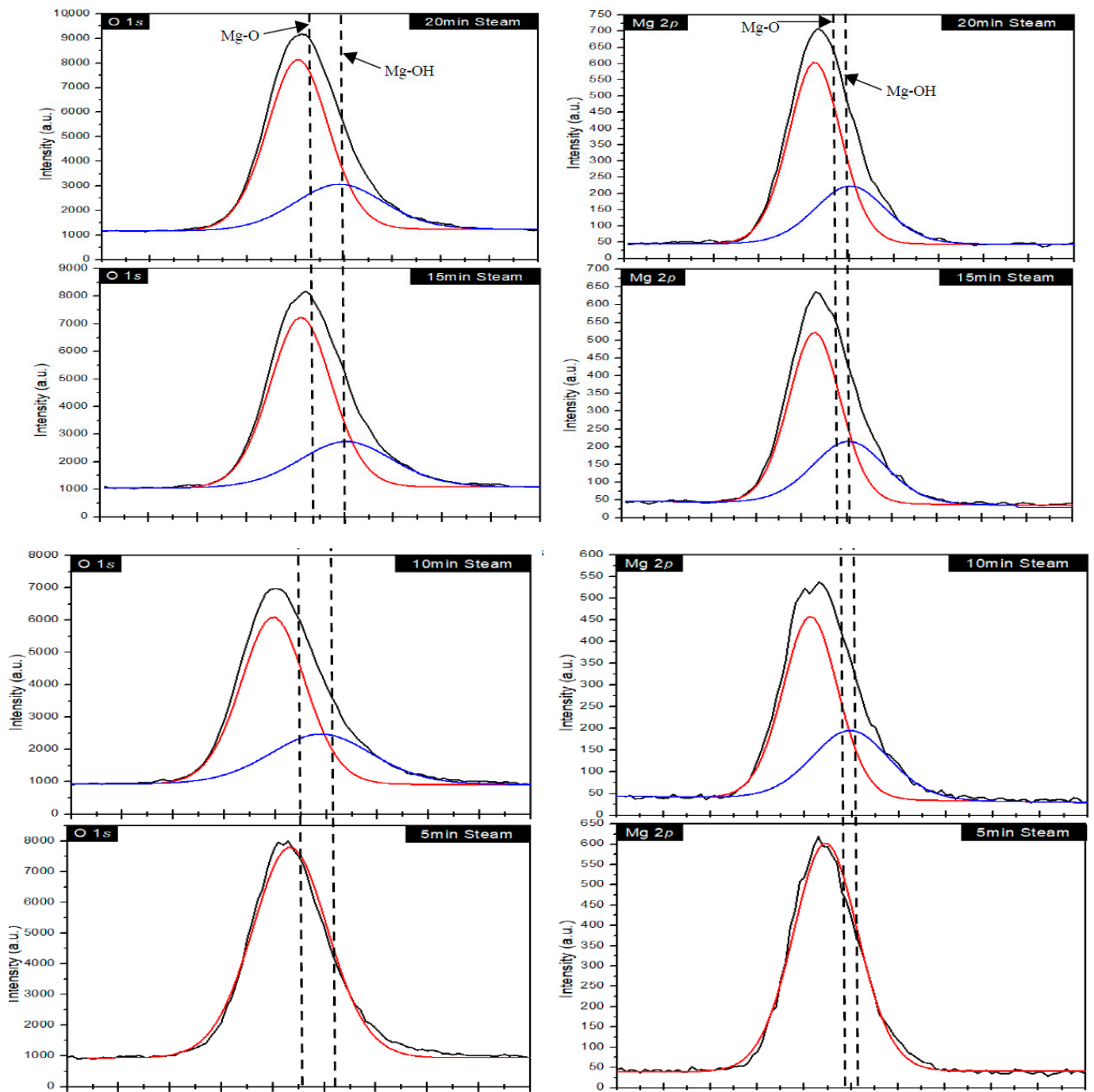


Figure 4. Cont.

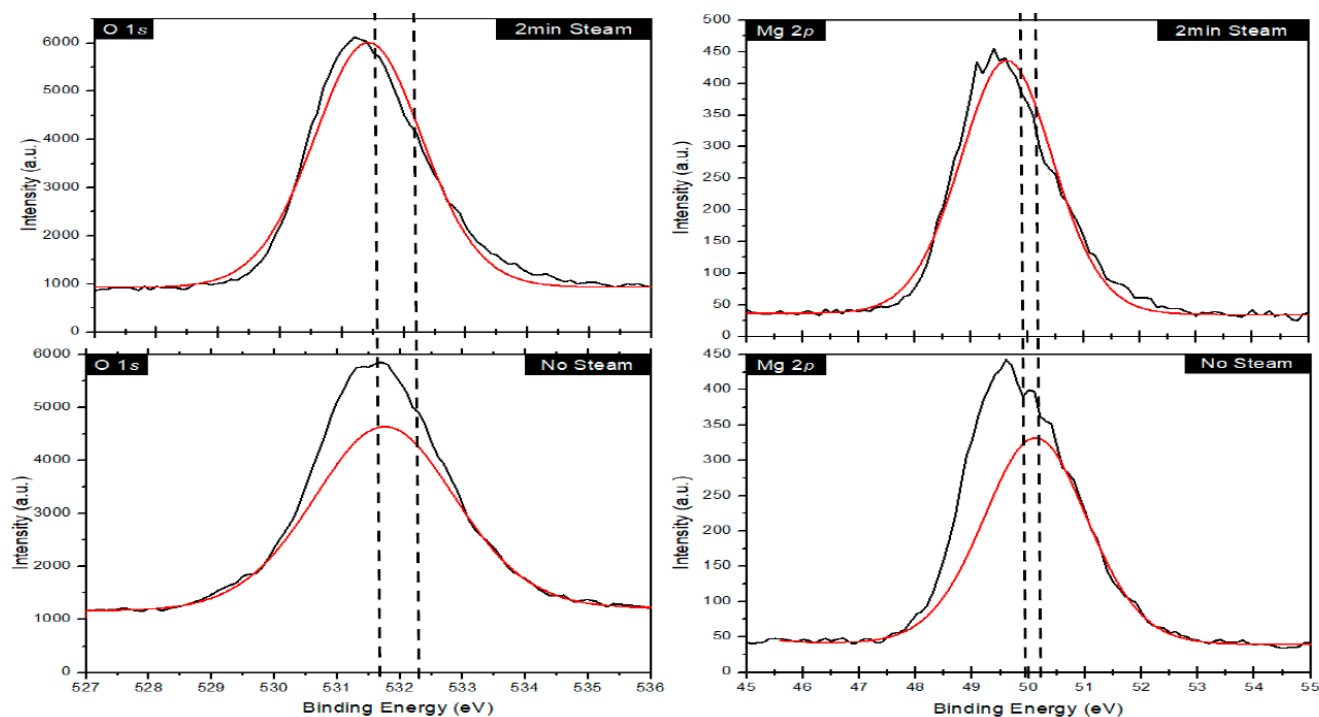


Figure 4. X-ray photoelectron spectra of the no-steamed and steamed samples. The no-steam sample is comprised of MgO, and the steamed samples at 100 °C show the formation of a MgO–Mg(OH)₂ composite structure.

To further analyze the effect to the surface area of the samples of steam exposure, BET analysis was carried out. The surface area and pore volume parameters of samples are shown in Table 1.

Table 1. Effect of hydration for surface area and pore volume parameters of samples.

Sample	Surface Area (m ² /g)	Total Pore Volume (cm ³ /g)	Avg Pore Size (nm)
No Steam	46.76	0.156	13.35
2	8.91	0.075	33.87
5	27.67	0.160	23.17
10	14.67	0.106	28.84
15	47.02	0.300	25.56
20	52.59	0.295	22.47

Before exposing steam (no-steam) to the samples, they showed a high surface area yet a lower average pore size. This could be a reason for the low CO₂ adsorption for the samples at 30 °C. However, once the samples were exposed to steam and with increased steaming time, the surface area of the samples showed a relative increment, which may have been due to the formation of valley-like structures observed in SEM analysis. The lower surface area of 2-min and 10-min steam exposed samples could be due to blocking of H₂O inside the pores, which would have impaired CO₂ chemisorption onto the MgO–Mg(OH)₂ composites. However, Wu et al. [25] just published a theoretical analysis that shows how the presence of H₂O considerably improves CO₂ adsorption by MgO. In addition to the polarization caused by charge transfer from the MgO surface, the electron localization to O and C atoms inside the CO₂ molecule results in further polarization of the CO₂ molecule. Furthermore, the longer the sample is exposed to steam, the more Mg(OH)₂ is produced, preventing the formation of a continuous MgCO₃ cell, which would impede CO₂ diffusion [29]. According to Siauciunas et al. [30], the rate of CO₂ chemisorption is affected by the amount of water in the bermorite. At low pressure conditions, Yong and

Rodrigues [31] found that a low water/steam concentration can boost the CO₂ adsorption ability of hydrotalcite-like compounds.

5. Conclusions

In this research, we present an experimental study on the morphology control of MgO–Mg(OH)₂ composite materials for effective CO₂ adsorption at 30 °C. The experimental data show that the CO₂ adsorption at 30 °C was improved from 2.43 wt.% to an impressive 4.12 wt.% with only 20 min by steaming time the original sample. This is due to the formation of Mg(OH)₂, where in the study the carbonate creation and breakdown processes were controlled and optimized. These findings hint at a new method and procedure for CO₂ adsorption that could lead to new CO₂ capture, mineralization, and fuel synthesis possibilities. By optimizing the crucial parameters such as steam duration and the calcination temperature, we aim to tune samples to improve the CO₂ capture capacity.

Author Contributions: Conceptualization, P.W. and H.L.S.; methodology H.L.S.; validation, H.L.S., W.P.C.L. and S.W.; investigation, H.L.S.; data curation, H.L.S.; writing—original draft preparation, P.W. and H.L.S.; writing—review and editing, P.W., S.W. and W.P.C.L. All authors have read and agreed to the published version of the manuscript.

Funding: This research was financially supported by Ministry of Education (Singapore), under the Tier 2 program (Award No. MOE2018-T2-1-163), and by the Agency for Science, Technology, and Research (A*STAR) (Singapore), under AME Individual Research Grant (Award No. A20E7c0108).

Institutional Review Board Statement: Not applicable.

Informed Consent Statement: Not applicable.

Data Availability Statement: The data presented in this study are available upon request from the corresponding author.

Conflicts of Interest: The authors declare no conflict of interest.

References

1. Hu, Y.; Guo, Y.; Sun, J.; Li, H.; Liu, W. Progress in MgO sorbents for cyclic CO₂ capture: A comprehensive review. *J. Mater. Chem. A* **2019**, *7*, 20103–20120. [[CrossRef](#)]
2. Pilarska, A.A.; Klapiszewski, L.; Jesionowski, T. Recent development in the synthesis, modification and application of Mg(OH)₂ and MgO: A review. *Powder Technol.* **2017**, *319*, 373–407. [[CrossRef](#)]
3. Johnson, I.; Liu, H. A study on factors affecting the degradation of magnesium and a magnesium-yttrium alloy for biomedical applications. *PLoS ONE* **2013**, *8*, e65603. [[CrossRef](#)] [[PubMed](#)]
4. Wetteland, C.L.; de Jesus Sanchez, J.; Silken, C.A.; Nguyen, N.-Y.T.; Mahmood, O.; Liu, H. Dissociation of magnesium oxide and magnesium hydroxide nanoparticles in physiologically relevant fluids. *J. Nanopart. Res.* **2018**, *20*, 1–17. [[CrossRef](#)]
5. Jose, N.; Ahmed, H.; Miguel, B.; Luis, E.; Jorge, B. Magnesia (MgO) Production and Characterization, and Its Influence on the Performance of Cementitious Materials: A Review. *Materials* **2020**, *13*, 4752. [[CrossRef](#)]
6. Chintareddy, V.R.; Lakshmi Kantam, M. Recent Developments on Catalytic Applications of Nano-Crystalline Magnesium Oxide. *Catal. Surv. Asia* **2011**, *15*, 89–110. [[CrossRef](#)]
7. Li, X.; Su, H.; Ren, G.; Wang, S. The role of MgO in the performance of Pd/SiO₂/cordierite monolith catalyst for the hydrogenation of 2-ethyl-anthraquinone. *Appl. Catal. A Gen.* **2016**, *517*, 168–175. [[CrossRef](#)]
8. Chen, Y.; Feng, Z.; Zhang, W. Effect of MgO Content on Mechanical Properties of Directionally Solidified Pure Magnesium. *Mater. Res.* **2021**, *24*. [[CrossRef](#)]
9. Han, K.K.; Zhou, Y.; Chun, Y.; Zhu, J.H. Efficient MgO-based mesoporous CO₂ trapper and its performance at high temperature. *J. Hazard Mater.* **2012**, *203–204*, 341–347. [[CrossRef](#)]
10. Julkapli, N.M.; Bagheri, S. Magnesium oxide as a heterogeneous catalyst support. *Rev. Inorg. Chem.* **2016**, *36*, 1–41. [[CrossRef](#)]
11. Cubukcuoglu, B.; Ouki, S.K. Solidification/stabilisation of electric arc furnace waste using low grade MgO. *Chemosphere* **2012**, *86*, 789–796. [[CrossRef](#)]
12. Ruhaimi, A.H.; Aziz, M.A.A.; Jalil, A.A. Magnesium oxide-based adsorbents for carbon dioxide capture: Current progress and future opportunities. *J. CO₂ Util.* **2021**, *43*, 101357. [[CrossRef](#)]
13. Elvira, G.B.; Francisco, G.C.; Victor, S.M.; Alberto, M.R. MgO-based adsorbents for CO₂ adsorption: Influence of structural and textural properties on the CO₂ adsorption performance. *J. Environ. Sci.* **2017**, *57*, 418–428. [[CrossRef](#)] [[PubMed](#)]
14. Bhagiyalakshmi, M.; Lee, J.Y.; Jang, H.T. Synthesis of mesoporous magnesium oxide: Its application to CO₂ chemisorption. *Int. J. Greenh. Gas Control* **2010**, *4*, 51–56. [[CrossRef](#)]

15. Ho, K.; Jin, S.; Zhong, M.; Vu, A.-T.; Lee, C.-H. Sorption capacity and stability of mesoporous magnesium oxide in post-combustion CO₂ capture. *Mater. Chem. Phys.* **2017**, *198*, 154–161. [[CrossRef](#)]
16. Taglieri, G.; Felice, B.; Daniele, V.; Ferrante, F. Mg(OH)₂ nanoparticles produced at room temperature by an innovative, facile, and scalable synthesis route. *J. Nanopart. Res.* **2015**, *17*, 1–13. [[CrossRef](#)]
17. Beall, G.W.; Duraia, E.-S.M.; El-Tantawy, F.; Al-Hazmi, F.; Al-Ghamdi, A.A. Rapid fabrication of nanostructured magnesium hydroxide and hydromagnesite via microwave-assisted technique. *Powder Technol.* **2013**, *234*, 26–31. [[CrossRef](#)]
18. Wu, J.; Yan, H.; Zhang, X.; Wei, L.; Liu, X.; Xu, B. Magnesium hydroxide nanoparticles synthesized in water-in-oil microemulsions. *J. Colloid Interface Sci.* **2008**, *324*, 167–171. [[CrossRef](#)] [[PubMed](#)]
19. Baidukova, O.; Skorb, E.V. Ultrasound-assisted synthesis of magnesium hydroxide nanoparticles from magnesium. *Ultrason. Sonochem.* **2016**, *31*, 423–428. [[CrossRef](#)] [[PubMed](#)]
20. Song, X.; Sun, S.; Zhang, D.; Wang, J.; Yu, J. Synthesis and characterization of magnesium hydroxide by batch reaction crystallization. *Front. Chem. Sci. Eng.* **2011**, *5*, 416–421. [[CrossRef](#)]
21. Xing, Z.; Bai, L.; Ma, Y.; Wang, D.; Li, M. Mechanism of Magnesium Oxide Hydration Based on the Multi-Rate Model. *Materials* **2018**, *11*, 1835. [[CrossRef](#)]
22. Thomas, J.J.; Musso, S.; Prestini, I.; Troczynski, T. Kinetics and Activation Energy of Magnesium Oxide Hydration. *J. Am. Ceram. Soc.* **2014**, *97*, 275–282. [[CrossRef](#)]
23. Parker, A.R.; Lawrence, C.R. Water capture by a desert beetle. *Nature* **2001**, *414*, 33–34. [[CrossRef](#)]
24. Hamilton, W.J.; Seely, M.K. Fog basking by the Namib Desert beetle, *Onymacris unguicularis*. *Nature* **1976**, *262*, 284–285. [[CrossRef](#)]
25. Wu, S.; Tan, B.T.; Senevirathna, H.L.; Wu, P. Polarization of CO₂ for improved CO₂ adsorption by MgO and Mg(OH)₂. *Appl. Surf. Sci.* **2021**, *562*, 150187. [[CrossRef](#)]
26. Senevirathna, H.L.; Lebedev, A.; Chen, V.Y.; Chou, C.-S.; Wu, P. Synthesis, characterization, CO₂ mineralization in air, and thermal decomposition of nano- C₈H₁₀MgO₁₀·4H₂O powder. *J. Environ. Manag.* **2021**, *295*, 3095. [[CrossRef](#)]
27. Jin, S.; Bang, G.; Lee, C.-H. Unusual morphology transformation and basicity of magnesium oxide controlled by ageing conditions and its carbon dioxide adsorption. *J. CO₂ Util.* **2020**, *41*, 1273. [[CrossRef](#)]
28. Liu, J.; Chen, F.; Yang, W.; Guo, J.; Xu, G.; Jia, F.; Shi, L. Excess soluble alkalis to prepare highly efficient MgO with relative low surface oxygen content applied in DMC synthesis. *Sci. Rep.* **2021**, *11*, 20931. [[CrossRef](#)]
29. Fricker, K.J.; Park, A.-H.A. Effect of H₂O on Mg(OH)₂ carbonation pathways for combined CO₂ capture and storage. *Chem. Eng. Sci.* **2013**, *100*, 332–341. [[CrossRef](#)]
30. Siauciunas, R.; Rupsyt, E.; Kitrys, S.; Galeckas, V. Influence of tobermorite texture and specific surface area on CO₂ chemisorption. *Colloids Surf. A Physicochem. Eng. Asp.* **2004**, *244*, 197–204. [[CrossRef](#)]
31. Yong, Z.; Rodrigues, A.r.E. Hydrotalcite-like compounds as adsorbents for carbon dioxide. *Energy Convers. Manag.* **2002**, *43*, 1865–1876. [[CrossRef](#)]